10.24425/acs.2020.133501

Archives of Control Sciences
Volume 30(LXVI), 2020
No. 2, *pages* 295–324

Vibration control and performance analysis of full car active suspension system using fractional order terminal sliding mode controller

T. YUVAPRIYA, P. LAKSHMI and S. RAJENDIRAN

The main goal of introducing Active Suspension System in vehicles is to reduce the vehicle body motion under road obstacles which improves the ride comfort of the passenger. In this paper, the Full Car Model (FCM) with seven Degrees of Freedom is considered and simulated by MATLAB/Simulink. The Terminal Sliding Mode Controller (TSMC) and Fractional Order Terminal Sliding Mode Controller (FOTSMC) are designed to enhance the ride quality, stability and passenger comfort for FCM. The designed FOTSMC has the ability to provide higher control accuracy in a finite time. The performances of the designed controllers are evaluated by measuring the vehicle body vibration in both angular and vertical direction under bump input and ISO-8608 random input against passive suspension system. The Frequency Weighted Root Mean Square (FWRMS) and Vibration dose value of Body Acceleration as per ISO-2631 are evaluated for FOTSMC, TSMC and PSS. The stability of the FCM is proved by Lyapunouv theory. Further analysis with sprung mass and speed variation of FCM demonstrate the robustness of proposed controller. To investigate the performances of designed controllers, comparison is made with existing Sliding Mode Controller (SMC) which proves that the designed FOTSMC performs better than existing SMC.

Key words: active suspension system, fractional order terminal sliding mode controller, ISO8608, ISO2631, stability analysis, vibration dose value

1. Introduction

In recent years Active Suspension System in the automotive industry plays an important role to achieve travelling comfort and road holding performances.

T. Yuvapriya (Corresponding Author, E-mail: tyuvapriya3@gmail.com) and P. Lakshmi (E-mail: p_lakshmi@annauniv.edu) are with Department of Electrical and Electronics Engineering, CEG, Anna University, Chennai, 600 025 India.

S. Rajendiran (E-mail: pecraja@gmail.com) is with Department of Electronics and Instrumentation Engineering, Pondicherry Engineering College, Puduchery, 605 014 India.

Received 6.7.2019. Revised 4.02.2020 and 14.04.2020.

The nonlinear Quarter Car Model(QCM) with time delay is considered to design a Proportional Integral Derivative (PID) control algorithm which establishes more accurate and precise suspension system [1]. The state dependent Riccatti equation is utilized for vibration control of QCM with sinusoidal bump and road roughness disturbances [2]. The adaptive optimal control method demonstrates the better performance in the presence of parametric uncertainties for QCM [3]. To minimise the tracking error and improve the stability of the vehicle at high speed, PID control technique is developed for ASS [4]. The introduction of the Fractional Order Fuzzy Sliding Mode Controller is to eliminate chattering effect in QCM with integrated seat suspension [5]. A self-tuning PID based Fuzzy Logic Controller(FLC) is developed for Half Car Model(HCM) especially when the parameters are changing and to cancel out road disturbances which improves the ride comfort [6]. The pseudo excitation method is considered to analyse the random vibration of an HCM at different speed and with different nonlinear levels of suspension spring [7]. For better disturbance rejection, optimised static output feedback control strategy is implemented to decrease vertical acceleration of HCM [8]. Generally practical ASS has parametric uncertainties and it can be rectified by adaptive tracking control method [9]. In order to effectively suppress the vibration of the vehicle, preview controller [10], GA tuned distance based fuzzy sliding mode controller [11] and Multiplexed model predictive controller [12] are designed for ASS. A model free adaptive Sliding Mode Controller (SMC) with fuzzy compensation technique significantly reduces the sprung mass acceleration [13]. The robustness and stability of the vehicle can be achieved with SMC under uneven road conditions [14]. The overall suspension system performances are stabilised by linear quadratic regulator and FLC when compared to PSS [15]. To achieve higher control accuracy and robustness, a novel kidney inspired algorithm with Terminal SMC (TSMC) is employed for Full Car Model (FCM) [16]. An observer based Fuzzy (FSMC) [17] and an evolutionary based FLC [18] has been developed to reduce the vibration level to zero for FCM. An accurate assessment of chattering phenomenon and SMC design solutions are discussed [19]. The fault tolerant control based optimal SMC is introduced to stabilize the chassis against uncertainties [20].

The adaptive control technique is introduced for the stabilisation of pitch and heave motions of HCM with back stepping and lyapunouv's stability theory [21]. To handle parameter uncertainties and time varying input delay, robust state feedback controller is developed for ASS [22]. The actuator failure is the main drawback in automotive field and it can be solved by fuzzy fault tolerant control technique [23]. Vibration isolator is discussed to minimise vibration in mass spring and damper system [24]. The cuckoo search optimisation [25] and Fuzzy PID technique [26] is addressed to enhance the ride comfort and stability of the Semi ASS. The nonlinear characteristics of electro hydraulic actuator are considered to achieve accurate control of FCM using adaptive robust control

method [27]. A motion mode energy method is presented to determine the energy contribution in FCM [28].

In this study, FOTSMC and TSMC are simulated for FCM. This paper presents Full vehicle model in section 2. In Section 3, the design of controllers is proposed. The simulation results and the robustness of the proposed controller are analyzed with variation of sprung mass and speed to illustrate the efficacy of the controllers in Section 4. The conclusions are outlined in Section 5.

2. Full car model

The full vehicle model with seven DOF [29–32] is shown in Fig. 1. It has sprung mass, unsprung masses of rear and front are represented by m_s, m_{ur} and m_{uf} respectively. The actuators are mounted in between the unsprung and sprung mass of each wheel. It generate bidirectional force between the body and the axle. The Control force, spring constants, damping coefficients, displacemnets and distance are represented as f, k, b, x and l respectively. The subscripts s, u, fr, fl, rr, rl are representing the sprung, unsprung, front right, front left, rear right and rear left respectively.

The sprung mass of FCM is considered to be a rigid body. It has freedom of motion in the vertical, roll and pitch directions. The vertical displacement at the centre of gravity is x_1, θ is the pitch angle and Φ is the roll angle of the sprung mass. The freedom of motion for each unsprung mass in the vertical direction such as x_{2fl}, x_{2rl}, x_{2fr} and x_{2rr}. The mathematical eqaution representing the FCM is from [33].

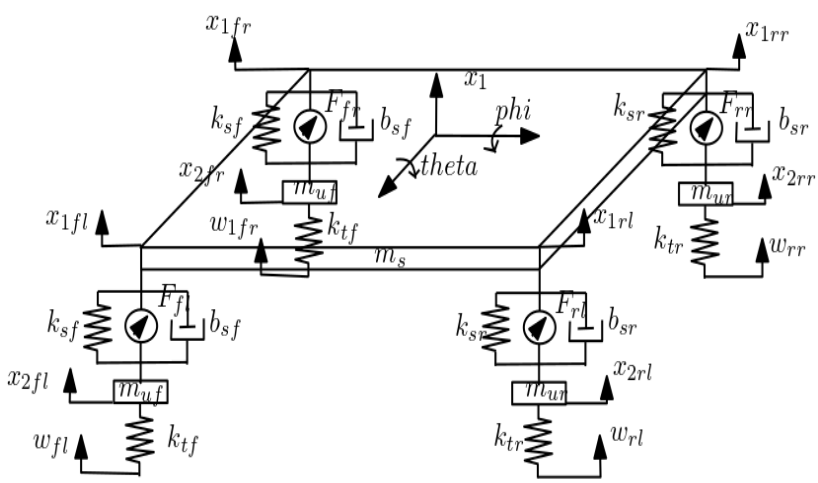

Figure 1: Full car model

The heave motion of sprung mass is

$$\begin{aligned} m_s\ddot{x}_1 = \Big[&k_{sf}\left(-x_{1_{fl}}-x_{1_{fr}}+x_{2_{fl}}+x_{2_{fr}}\right) + k_{sr}\left(-x_{1_{rl}}-x_{1_{rr}}+x_{2_{rl}}+x_{2_{rr}}\right) \\ &+ b_{sf}\left(-\dot{x}_{1_{fl}}-\dot{x}_{1_{fr}}+\dot{x}_{2_{fl}}+\dot{x}_{2_{fr}}\right) + b_{sr}\left(-\dot{x}_{1_{rl}}-\dot{x}_{1_{rr}}+\dot{x}_{2_{rl}}+\dot{x}_{2_{rr}}\right) \\ &+ f_{fl} + f_{fr} + f_{rl} + f_{rr}\Big]. \end{aligned} \tag{1}$$

The pitch motion of sprung mass is

$$\begin{aligned} I_\theta\ddot{\theta} = \Big[&k_{sf}l_f\left(-x_{1_{fl}}-x_{1_{fr}}+x_{2_{fl}}+x_{2_{fr}}\right) - k_{sr}l_r\left(-x_{1_{rl}}-x_{1_{rr}}+x_{2_{rl}}+x_{2_{rr}}\right) \\ &+ b_{sf}l_f\left(-\dot{x}_{1_{fl}}-\dot{x}_{1_{fr}}+\dot{x}_{2_{fl}}+\dot{x}_{2_{fr}}\right) - b_{sr}l_r\left(-\dot{x}_{1_{rl}}-\dot{x}_{1_{rr}}+\dot{x}_{2_{rl}}+\dot{x}_{2_{rr}}\right) \\ &- l_f f_{fl} - l_f f_{fr} + l_r f_{frl} + l_r f_{rr}\Big]. \end{aligned} \tag{2}$$

The roll motion of sprung mass is

$$\begin{aligned} I_\phi\ddot{\Phi} = \Big[&k_{sf}t_f\left(-x_{1_{fl}}+x_{1_{fr}}+x_{2_{fl}}-x_{2_{fr}}\right) + k_{sr}t_r\left(-x_{1_{rl}}+x_{1_{rr}}+x_{2_{rl}}-x_{2_{rr}}\right) \\ &+ b_{sf}t_f\left(-\dot{x}_{1_{fl}}+\dot{x}_{1_{fr}}+\dot{x}_{2_{fl}}-\dot{x}_{2_{fr}}\right) + b_{sr}t_r\left(-\dot{x}_{1_{rl}}+\dot{x}_{1_{rr}}\dot{x}_{2_{rl}}-\dot{x}_{2_{rr}}\right) \\ &- t_f f_{fl} + t_f f_{fr} - t_r f_{rl} + t_r f_{rr}\Big]. \end{aligned} \tag{3}$$

Vertical deflection of front left wheel is

$$\begin{aligned} m_{uf}\ddot{x}_{2_{fl}} = -\Big[&k_{sf}\left(-x_{1_{fl}}+x_{2_{fl}}\right) + k_{tf}\left(x_{2_{fl}}-w_{fl}\right) \\ &+ b_{sf}\left(-\dot{x}_{1_{fl}}+\dot{x}_{2_{fl}}\right) - f_{fl}\Big]. \end{aligned} \tag{4}$$

Vertical deflection of front right wheel is

$$\begin{aligned} m_{uf}\ddot{x}_{2_{fr}} = -\Big[&k_{sf}\left(-x_{1_{fr}}+x_{2_{fr}}\right) + k_{tf}\left(x_{2_{fr}}-w_{fr}\right) \\ &+ b_{sf}\left(-\dot{x}_{1_{fr}}+\dot{x}_{2_{fr}}\right) - f_{fr}\Big]. \end{aligned} \tag{5}$$

Vertical deflection of rear left wheel is

$$m_{ur}\ddot{x}_{2_{rl}} = -\Big[k_{sr}\left(-x_{1_{rl}}+x_{2_{rl}}\right) + k_{tr}\left(x_{2_{rl}}-w_{rl}\right) + b_{sr}\left(-\dot{x}_{1_{rl}}+\dot{x}_{2_{rl}}\right) - f_{rl}\Big]. \tag{6}$$

Vertical deflection of rear right wheel is

$$\begin{aligned} m_{ur}\ddot{x}_{2_{rr}} = -\Big[&k_{sr}\left(-x_{1_{rr}}+x_{2_{rr}}\right) + k_{tr}\left(x_{2_{rr}}-w_{rr}\right) \\ &+ b_{sr}\left(-\dot{x}_{1_{rr}}+\dot{x}_{2_{rr}}\right) - f_{rr}\Big], \end{aligned} \tag{7}$$

where

$$x_{1_{fl}} = x_1 + t_f\Phi + l_f\theta, \tag{8}$$

$$x_{1_{fr}} = x_1 - t_f\Phi + l_f\theta, \tag{9}$$

$$x_{1_{rl}} = x_1 + t_f\Phi - l_f\theta, \tag{10}$$

$$x_{1_{rr}} = x_1 - t_f\Phi - l_f\theta. \tag{11}$$

3. Designs of controllers

The sliding mode control technique offers an effective approach to control time varying systems with disturbances and parameter variations. To reduce the chattering effect and settling time, FOTSMC is designed and simulated for FCM. The sliding surface is chosen as suspension deflection and car body velocity of each wheel to design FOTSMC. The control forces are given to each wheel of FCM which act against the vibration induced by road disturbances. The Lyapunov's function is chosen as $V = \frac{1}{2}s^2$ to design the SMC. The condition for SMC is

$$\dot{V} = s\dot{s} < 0, \tag{12}$$

where s is the sliding surface.

3.1. Design of terminal sliding mode controller

The chattering effect is introduced by SMC which detoriates the control performance. To weaken the chattering effect, the TSMC is designed to reduce the vibration and the system trajectories will finally arrive at the sliding surface in a finite time [16]. The system moves with the sliding mode at $s = 0$ as per equation (12).

The variation of speed and mass is carried out to test the convergence of TSMC [19].

To design the TSMC, the terminal sliding surface is chosen as follows

$$s = y_2^{p/q} + \lambda y_1, \tag{13}$$

where λ is the sliding surface gain. p and q are integers which satisfy the condition $1 < \frac{p}{q} < 2$ [34]. By differentiation

$$\dot{s} = \frac{p}{q} y_2^{\frac{p}{q}-1}\dot{y}_2 + \lambda\dot{y}_1 \tag{14}$$

as per the equation (12), the system moves on the sliding mode at $\dot{s} = 0$

$$0 = \frac{p}{q} y_2^{\frac{p}{q}-1} \dot{y}_2 + \lambda \dot{y}_1 , \tag{15}$$

$$0 = \dot{y}_2 + \frac{\lambda \dot{y}_1}{\frac{p}{q} y_2^{\frac{p}{q}-1}} \tag{16}$$

since $y_2 = \dot{y}_1$

$$0 = \dot{y}_2 + \lambda \frac{q}{p} (\dot{y}_1)^{2-\frac{p}{q}} . \tag{17}$$

3.2. Design of fractional order terminal sliding mode controller

The benefits of TSMC and fractional order SMC are motivating to design the FOTSMC. To design the FOTSMC, the fractional derivative term is included in the TSMC equations. The fast and accurate tracking can be achieved by designing a high precision robust FOTSMC control strategy for FCM with ASS. The FOTSMC has the ability to stabilise the tracking error to zero in a finite time. Also the chattering effect is eliminated by FOTSMC and it improves the ride comfort of the passenger. The robustness and stability of FCM can be guaranteed with FOTSMC.

Therefore, the fractional order terminal sliding surface is chosen by combining the fractional order derivative and terminal values of the power as follows [35],

$$s = (y_2)^{p/q} + \lambda y_1 . \tag{18}$$

Since $y_2 = \dot{y}_1$

$$s = (\dot{y}_1)^{p/q} + \lambda y_1 , \tag{19}$$

$$s = (D^{\alpha} y_1)^{p/q} + \lambda y_1 , \tag{20}$$

where D represents the Differentiation and α is the fractional order of the Differentiation (D)

$$s = \left(D^{\alpha} D^{-1} D^{1} y_1\right)^{p/q} + \lambda y_1 , \tag{21}$$

$$s = \left(D^{\alpha-1} \dot{y}_1\right)^{p/q} + \lambda y_1 . \tag{22}$$

By differentiation

$$\dot{s} = \frac{p}{q} \left(D^{\alpha-1} \dot{y}_1\right)^{\frac{p}{q}-1} D^{\alpha-1} \ddot{y}_1 + \lambda \dot{y}_1 , \tag{23}$$

$$\dot{s} = \frac{p}{q}\left(D^{\alpha-1}\right)^{\frac{p}{q}-1} D^{\alpha-1}\left(\dot{y}_1\right)^{\frac{p}{q}-1}\ddot{y}_1 + \lambda\dot{y}_1\,, \tag{24}$$

$$\dot{s} = \frac{p}{q}\left(D^{\alpha-1}\right)^{p/q}\left(\dot{y}_1\right)^{\frac{p}{q}-1}\ddot{y}_1 + \lambda\dot{y}_1 \tag{25}$$

as per the equation (12)

$$0 = \frac{p}{q}\left(D^{\alpha-1}\right)^{p/q}\left(\dot{y}_1\right)^{\frac{p}{q}-1}\ddot{y}_1 + \lambda\dot{y}_1\,. \tag{26}$$

Dividing the above equation by $\frac{p}{q}\left(D^{\alpha-1}\right)^{p/q}\left(\dot{y}_1\right)^{\frac{p}{q}-1}$ and subtituting $\ddot{y}_1 = \dot{y}_2$

$$0 = \dot{y}_2 + \lambda\frac{q}{p}\left(D^{1-\alpha}\right)^{p/q}\dot{y}_1^{2-\frac{p}{q}}. \tag{27}$$

3.3. Derivation of control forces

The suspension deflection and car body velocity are chosen as state variables to design actuator force for front left wheel. The suspension deflection for front left wheel is

$$y_1 = x_{1fl} - x_{2fl} \tag{28}$$

and car body velocity for front left wheel is

$$y_2 = \dot{x}_{1fl}\,. \tag{29}$$

These state variables y_1 and y_2 are substituted in Eq. (17), the control force for front left f_{fl} wheel for the TSMC is derived as

$$\begin{aligned} f_{fl} = &-k_{sf}\left(-x_{1_{fl}}-x_{1_{fr}}+x_{2_{fl}}+x_{2_{fr}}\right) - k_{sr}\left(-x_{1_{rl}}-x_{1_{rr}}+x_{2_{rl}}+x_{2_{rr}}\right)\\ &- b_{sf}\left(-\dot{x}_{1_{fl}}-\dot{x}_{1_{fr}}+\dot{x}_{2_{fl}}+\dot{x}_{2_{fr}}\right) - b_{sr}\left(-\dot{x}_{1_{rl}}-\dot{x}_{1_{rr}}+\dot{x}_{2_{rl}}+\dot{x}_{2_{rr}}\right)\\ &- f_{fr} - f_{rl} - f_{rr} - l_f m_s\ddot{\theta} - t_f m_s\ddot{\phi}\\ &- \lambda\frac{q}{p}m_s\left(\dot{x}_{1_{fl}}-\dot{x}_{2_{fl}}\right)^{2-\frac{p}{q}} - k\,\mathrm{sign}(s). \end{aligned} \tag{30}$$

Similarlly, the state variables y_1 and y_2 are substituted in the equation (27), the control force for front left f_{fl} wheel for the FOTSMC is derived as

$$\begin{aligned} f_{fl} = &-k_{sf}\left(-x_{1_{fl}}-x_{1_{fr}}+x_{2_{fl}}+x_{2_{fr}}\right) - k_{sr}\left(-x_{1_{rl}}-x_{1_{rr}}+x_{2_{rl}}+x_{2_{rr}}\right)\\ &- b_{sf}\left(-\dot{x}_{1_{fl}}-\dot{x}_{1_{fr}}+\dot{x}_{2_{fl}}+\dot{x}_{2_{fr}}\right) - b_{sr}\left(-\dot{x}_{1_{rl}}-\dot{x}_{1_{rr}}+\dot{x}_{2_{rl}}+\dot{x}_{2_{rr}}\right)\\ &- f_{fr} - f_{rl} - f_{rr} - l_f m_s\ddot{\theta} - t_f m_s\ddot{\phi}\\ &- \lambda\frac{q}{p}m_s\left(D^{1-\alpha}\right)^{p/q}\left(\dot{x}_{1_{fl}}-\dot{x}_{2_{fl}}\right)^{2-\frac{p}{q}} - k\,\mathrm{sign}(s), \end{aligned} \tag{31}$$

where $k\,\mathrm{sign}(s)$ is the switching function, k is the positive constants, which satisfies the desired criteria $s\dot{s} < 0$ and brings the system into the sliding surface then converges to zero.

Similarly, the other three control forces are derived with different state variables. They are as follows:

To design the control force in the front right wheel, the state variables are chosen as follows, suspension deflection of front right wheel $y_1 = x_{1fr} - x_{2fr}$, car body velocity of front Right wheel $y_2 = \dot{x}_{1fr}$.

To design the control force in the rear left wheel, the state variables are chosen as follows, suspension deflection of rear left wheel $y_1 = x_{1rl} - x_{2rl}$, car body velocity of rear left wheel $y_2 = \dot{x}_{1rl}$.

To design the control force in the rear right wheel, the state variables are chosen as follows, suspension deflection of rear right wheel $y_1 = x_{1rr} - x_{2rr}$, car body velocity of rear right wheel $y_2 = \dot{x}_{1rr}$.

All the four control forces are similar with its corresponding paramters.

4. Numerical simulation and results

In this section, FCM is considered for simulation and analyse the performances of designed controllers by applying two different road disturbances [33] such as Bump Input (BI) and Random Input (RI) (Fig. 2).

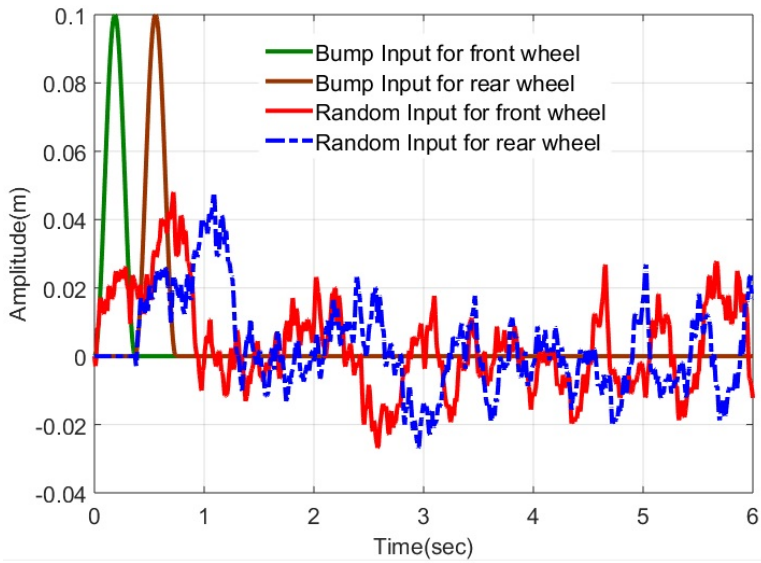

Figure 2: Road profiles

The Bump input is designed as per the following equation

$$z_r(t) = \begin{cases} \dfrac{a_1}{2}\left(1 - \cos\left(2\pi \dfrac{v_0}{l}\right)t\right) & \longrightarrow 0 \leqslant t \leqslant \dfrac{l}{v_0}, \\ 0 & \longrightarrow t \geqslant \dfrac{l}{v_0}, \end{cases} \tag{32}$$

where a_1 is the amplitude (0.1 m) and l is the length of the bump (2 m), v_0 is the vehicle speed (30 kmph).

The real roads are random in nature. The roads are modelled and classified by the ISO 8608 from very good road to very poor road based on the road roughness values. Therefore, random road with road roughness value can be modelled by passing a Gaussian white noise through a shaping filter.

$$\dot{z}_r(t) = -2\pi f_o z_r(t) + 2\pi\sqrt{(G_0 v_0)}\,\omega(t), \tag{33}$$

where $z_r(t)$ is road random, G_o is road roughness coefficient (for very poor road 256×10^{-6} ($\mathrm{m}^3\,\mathrm{cycle}^{-1}$)), v_0 is vehicle velocity (30 kmph), f_o is lower limit cut-off frequency of filter (0.01 Hz), $\omega(t)$ is Gaussian white noise.

The designed controllers are simulated using MATLAB 2012b/Simulink. The FCM parameters considered for simulation are from [33] and shown in Table 1.

Table 1: Parameters for FCM

Parameters	Value	Parameters	Value
m_s	1500 kg	m_{uf}, m_{ur}	59.59 kg
K_{sf}	35000 N/m	K_{sr}	38000 N/m
K_{tf}	190000 N/m	Ktr	190000 N/m
I_θ	2160 kg/m^2	I_Φ	460 kg/m^2
b_{sf}	1000 N/m	bsr	1100 N/m
T_f	0.505 m	T_r	0.557 m
l_f	1.4 m	l_r	1.7 m

The parameters used for simulation are chosen by trail and error method. They are, $p = 23$ and $q = 25$ for both TSMC and FOTSMC. The $\alpha = 0.85$ for FOTSMC. $\lambda = 0.9$, $K = 1$.

4.1. Analysis with bump input

The amplitude of BI for front and rear wheel is 0.1 m with a delay of 0.37 sec [33]. The passive response of BA, PA and RA for FCM are presented in Figs. 3–5 respectively. When the vehicle is subjected to BI, it affects the ride comfort of the

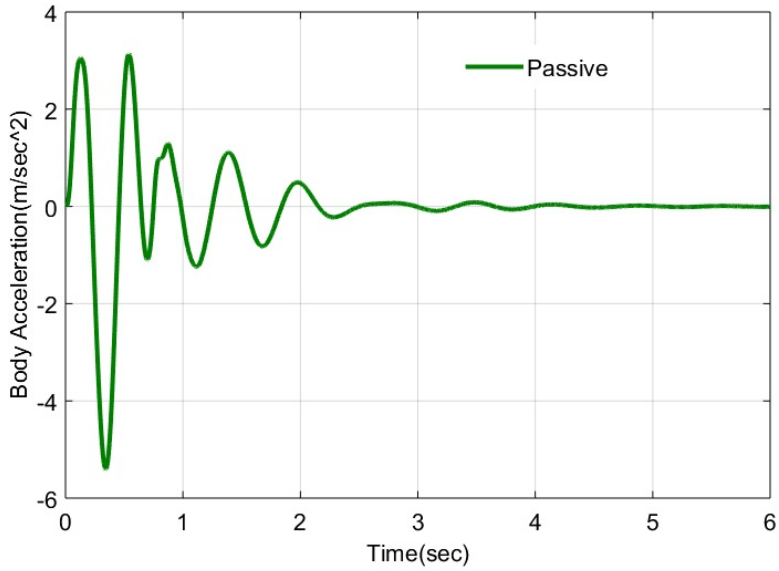

Figure 3: Passive response of FCM – BA – BI

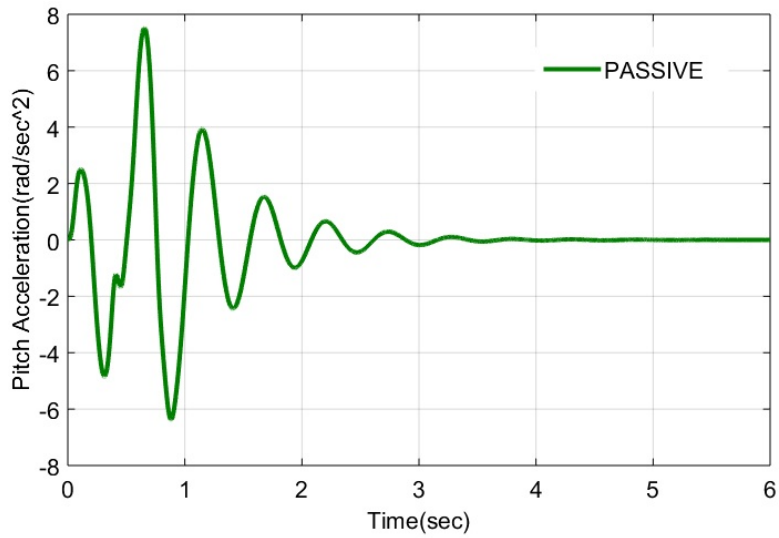

Figure 4: Passive response of FCM – PA – BI

passenger. Hence the maximum peak overshoot and settling time of BA, RA and PA are increased with PSS.

In order to investigate the ride comfort of the passenger, vibration of the vehicle body should be measured in angular and vertical (heave) direction. The

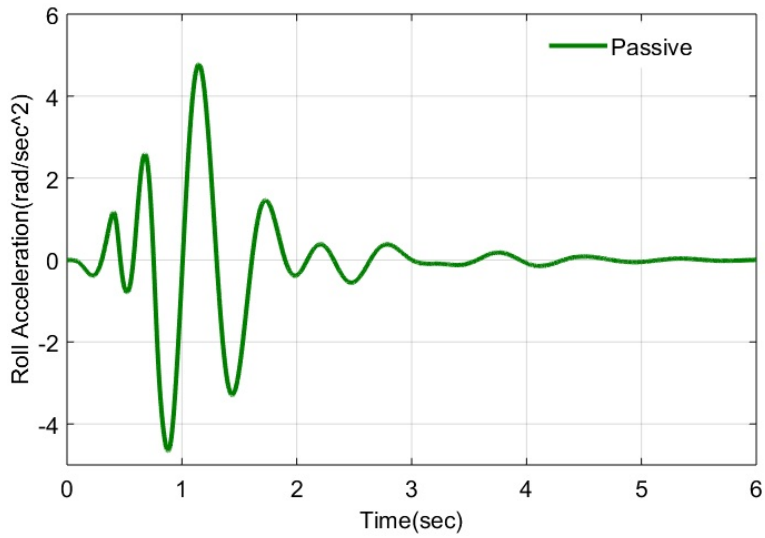

Figure 5: Passive response of FCM – RA – BI

control forces are generated for each wheel of FCM with BI by FOTSMC and TSMC. These forces act against the road disturbance and it reduces vibration. The BA, PA and RA responses are shown in Figs. 6–8 respectively.

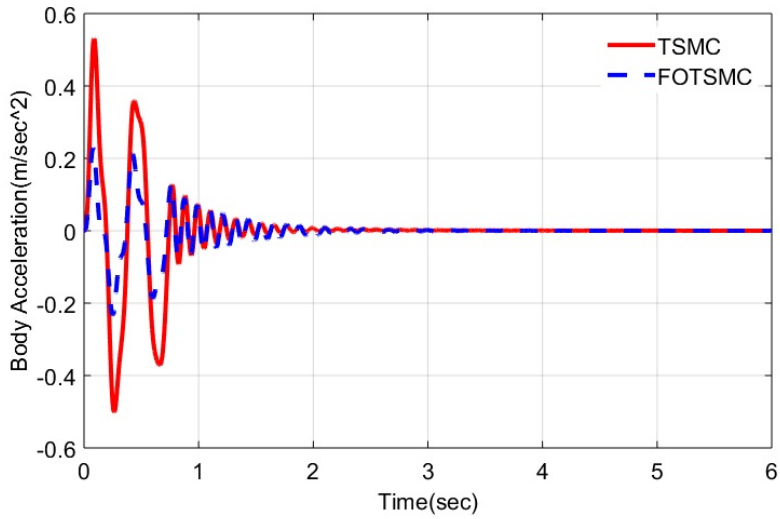

Figure 6: Reduction of BA by SMCs – BI

The maximum peak overshoot of TSMC with BA, PA and RA are 0.56 m/sec^2, 0.46 rad/sec^2 and 0.008 rad/sec^2 respectively. Similarly, for FOTSMC with BA,

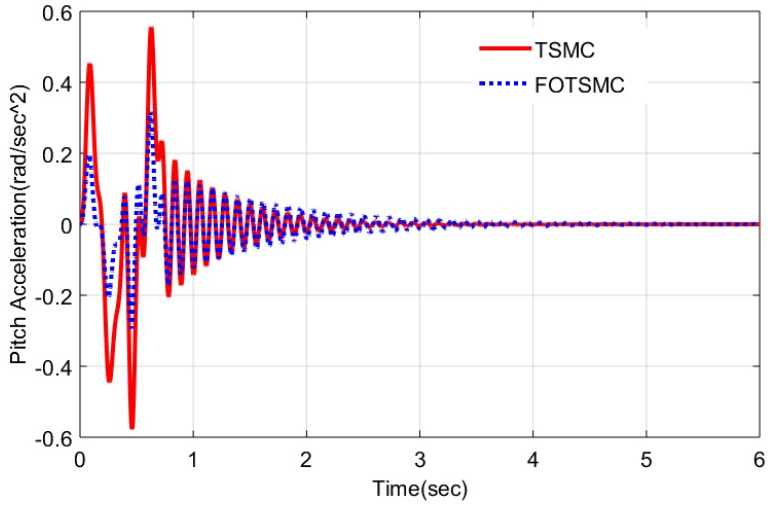

Figure 7: Reduction of PA by SMCs – BI

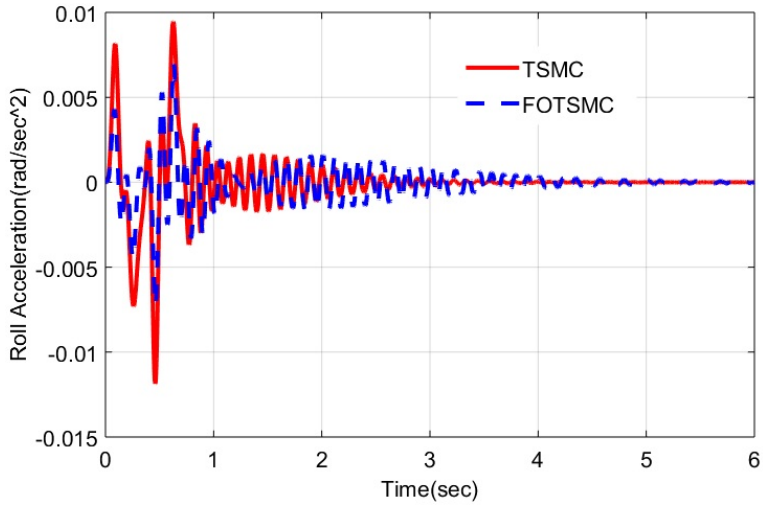

Figure 8: Reduction of RA by SMCs – BI

PA and RA are 0.22 m/sec^2, 0.2 rad/sec^2 and 0.0045 rad/sec^2 respectively. The comparative numerical value of maximum peak overshoot proves that level of vibration is significantly reduced with FOTSMC than TSMC.

The control forces for each wheel are produced by TSMC and FOTSMC are shown in Figs. 9–12 respectively. The FOTSMC takes more control action to reduce the vibration of FCM.

To evaluate the vibration reduction of the designed controllers, the RMS values with BI are computed. It is clear from the Table 2, the percentage of

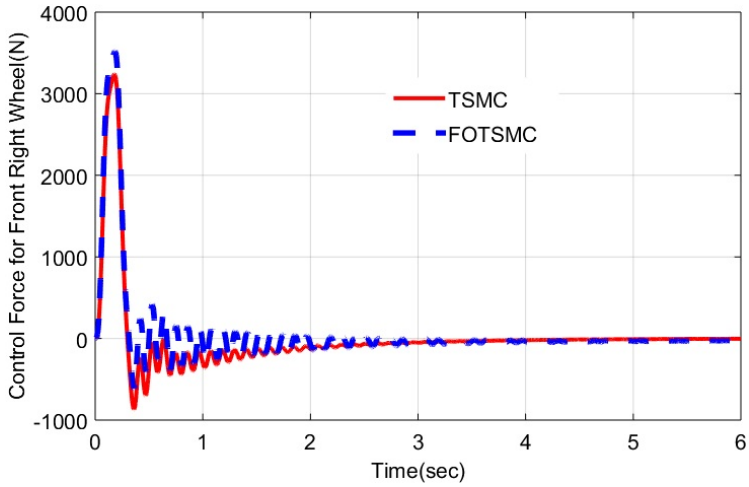

Figure 9: Force produced by the front right actuator – BI

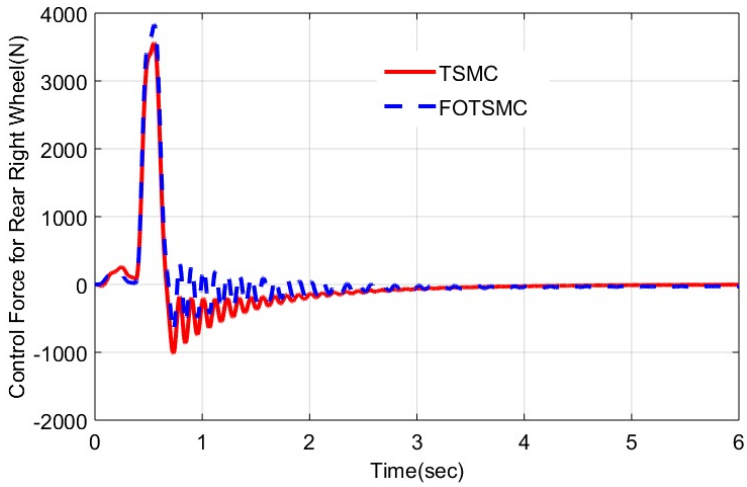

Figure 10: Force produced by the rear right actuator – BI

Table 2: Performance index of FCM

	BA (m/s^2)		PA (rad/s^2)		RA (rad/s^2)	
	BI	RI	BI	RI	BI	RI
PASSIVE	0.995	0.980	1.747	1.578	1.215	0.807
TSMC	0.151	0.500	0.150	0.715	0.003	0.215
FOTSMC	0.068	0.467	0.079	0.669	0.002	0.204

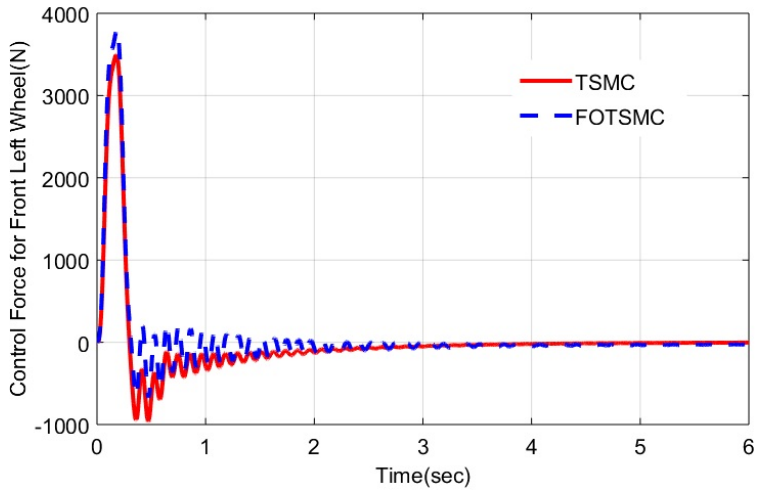

Figure 11: Force produced by the front left actuator – BI

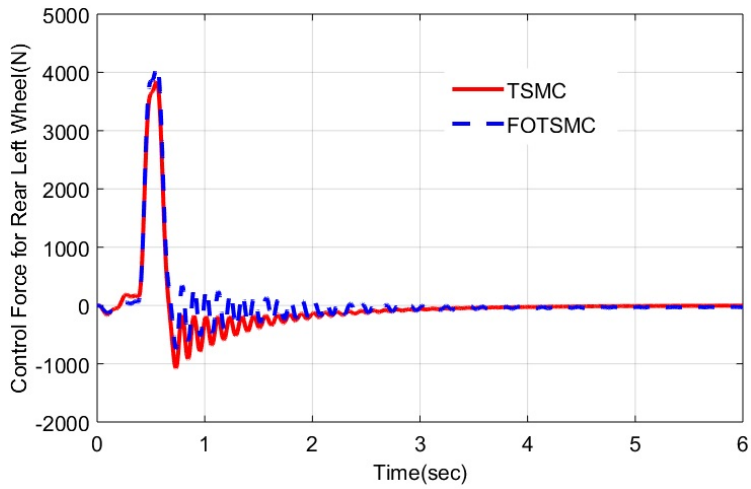

Figure 12: Force produced by the rear left actuator – BI

reduction in RMS values of BA, RA and PA are computed with respect to PSS. This sufficiently implies that TSMC with BI reduces RMS values of BA, RA and PA by 85%, 99% and 91.4% whereas FOTSMC reduces RMS values of BA, RA and PA by 93%, 99.7% and 95.4% respectively.

4.2. Analysis with random input

The Random road is designed as per ISO 8608 and used for simulation [33] and the vehicle speed is 30 Kmph. Figs. 13–15 shows the passive responses of

BA, PA and RA with RI. The maximum peak overshoot of BA, RA and PA are increased with PSS. The surface of the road is not in smooth condition. In order to examine the quality of the designed controllers, the RI is considered for analysis.

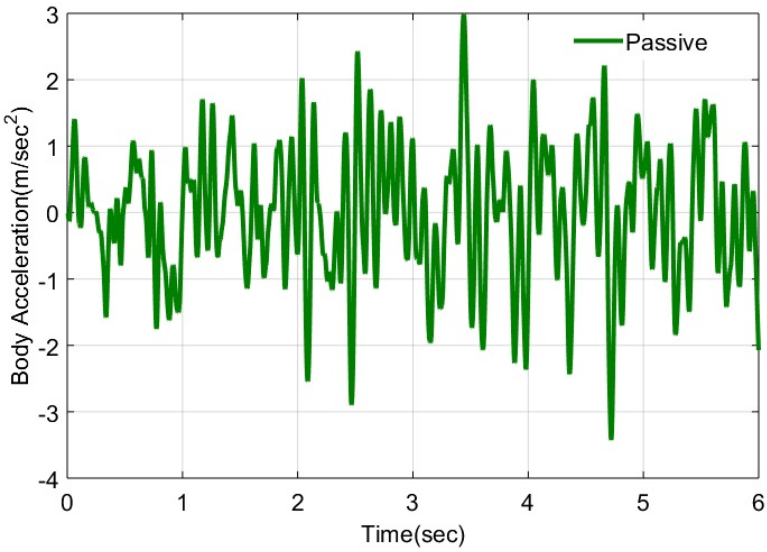

Figure 13: Passive response of FCM-BA-RI

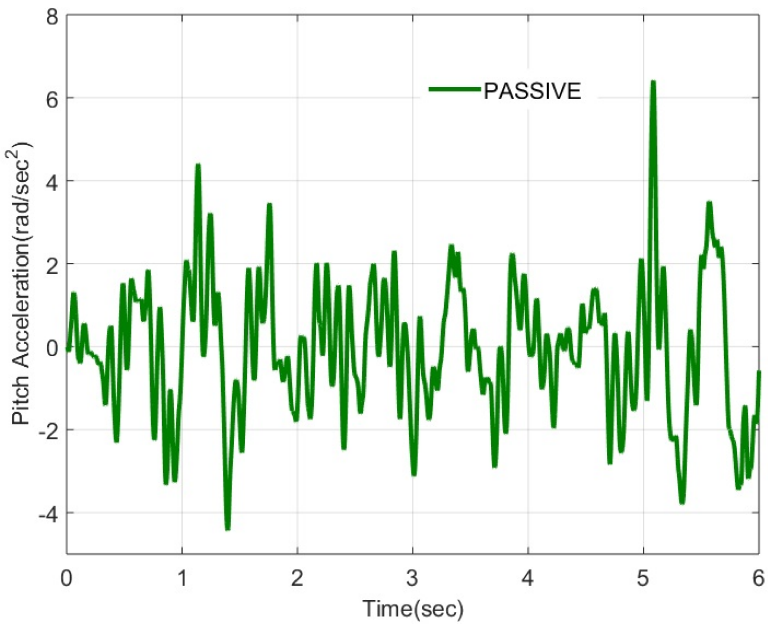

Figure 14: Passive response of FCM-PA-RI

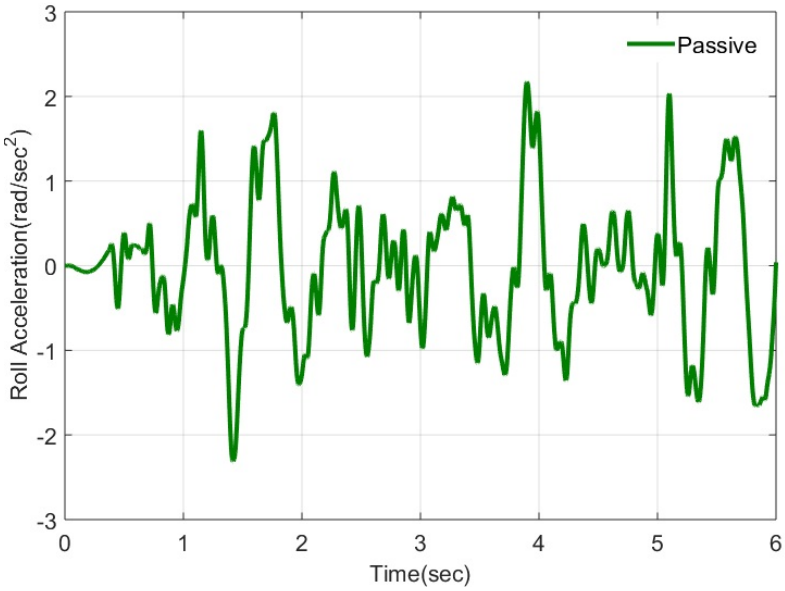

Figure 15: Passive response of FCM-RA-RI

Figs. 16–18 shows the ASS responses of BA, PA and RA with RI. It can be noticed from the figures that the RMS values of BA and maximum peak overshoot with RI are decreased by FOTSMC than TSMC and PSS. The control forces for each

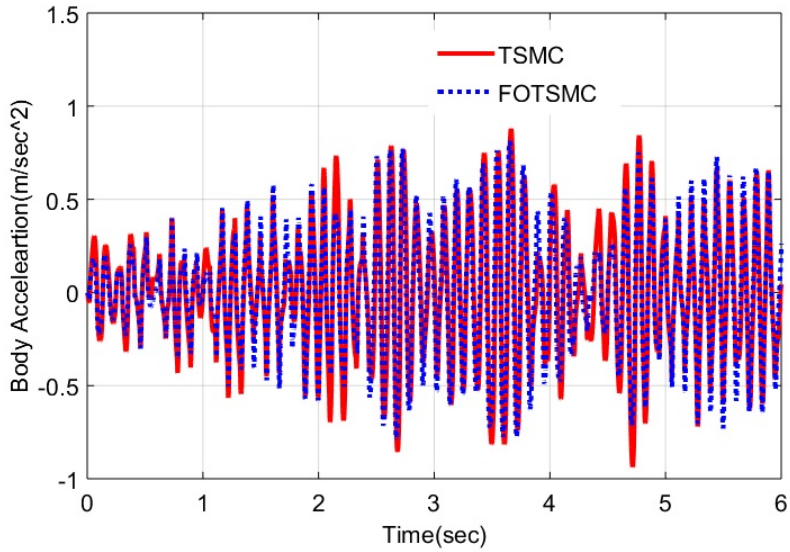

Figure 16: Reduction of BA by SMCs-RI

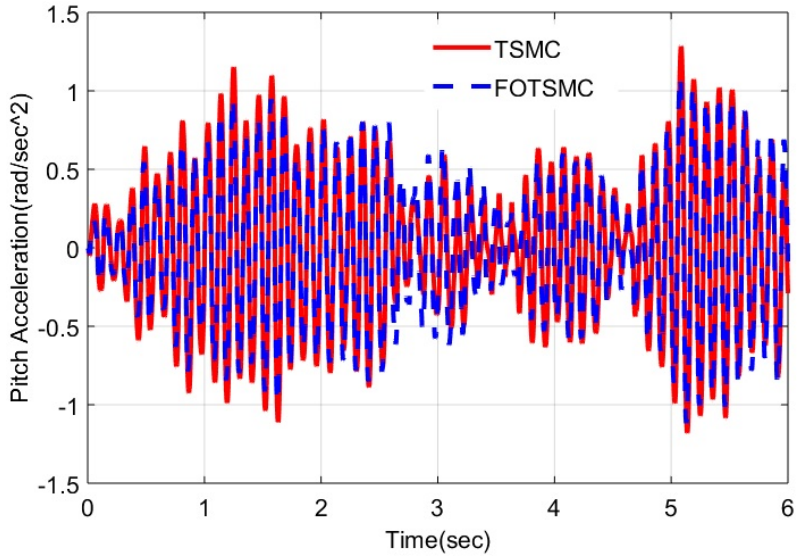

Figure 17: Reduction of PA by SMCs-RI

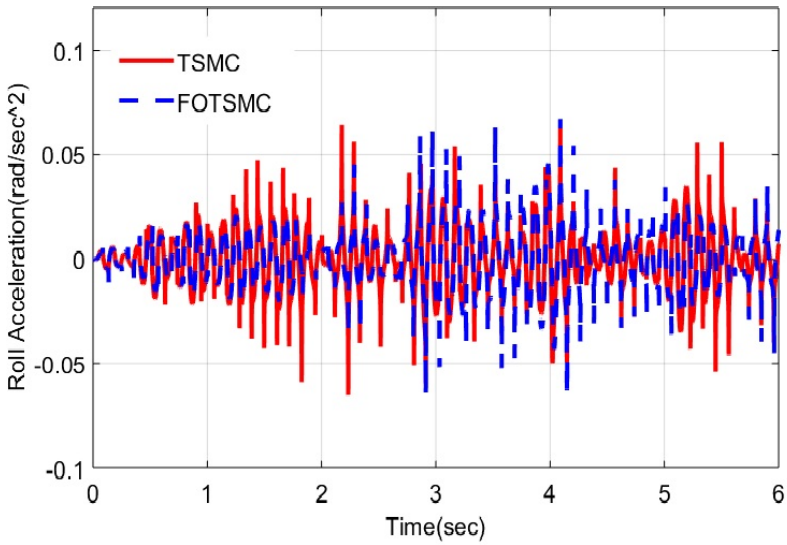

Figure 18: Reduction of RA by SMCs-RI

wheel for RI are shown in Figs. 19–22. The control forces generated from the FOTSMC and TSMC are used to suppress the vibration of FCM. The analysis indicates that the FOTSMC improves the angular and vertical accelerations of the FCM compared to TSMC and PSS.

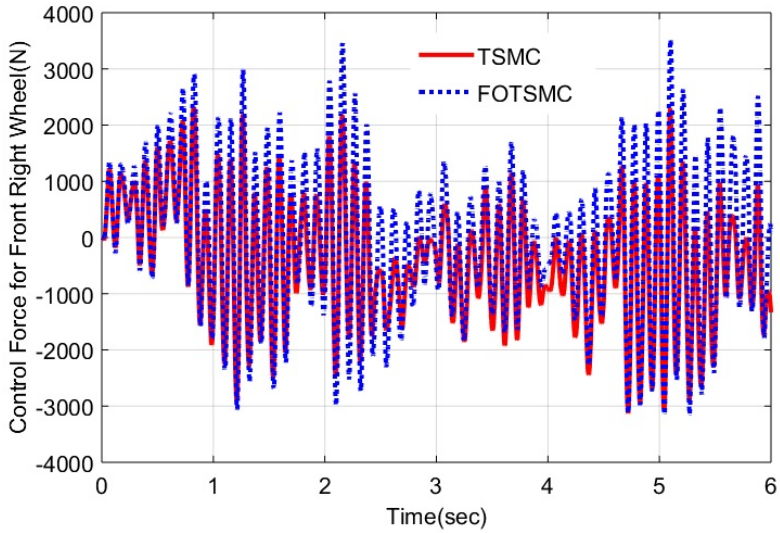

Figure 19: Force produced by the front right actuator – RI

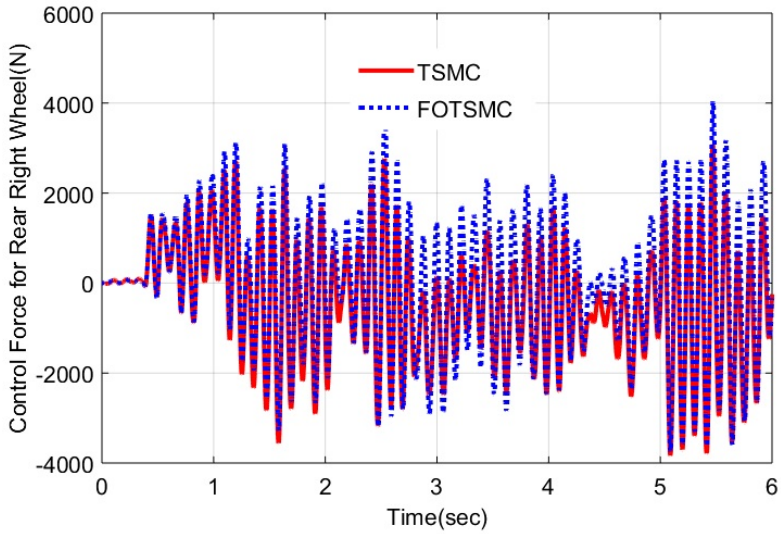

Figure 20: Force produced by the rear right actuator – RI

The RMS values of BA, PA and RA with TSMC are decreased by 48.5%, 54.6% and 73.3% while for FOTSMC gives 52.3%, 57.6% and 74% respectively. The comparative analysis with numerical simulation results shows that FOTSMC increases the percentage of reduction in RMS values of BA, PA and RA compared to TSMC and PSS.

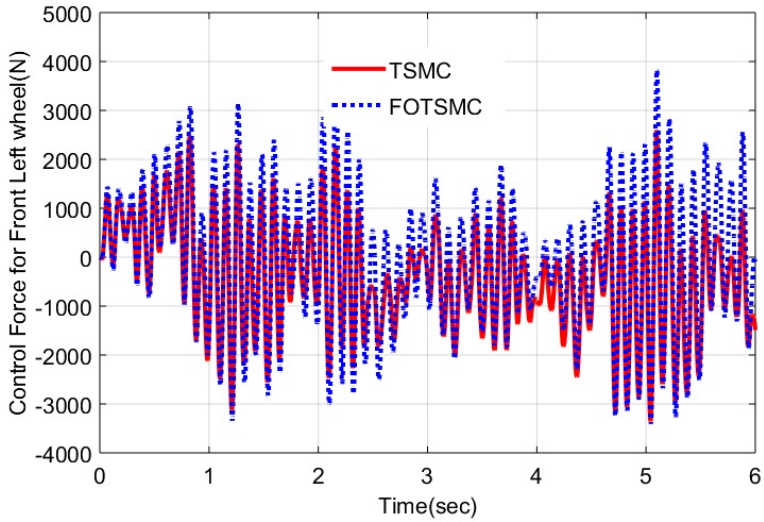

Figure 21: Force produced by the front left actuator – RI

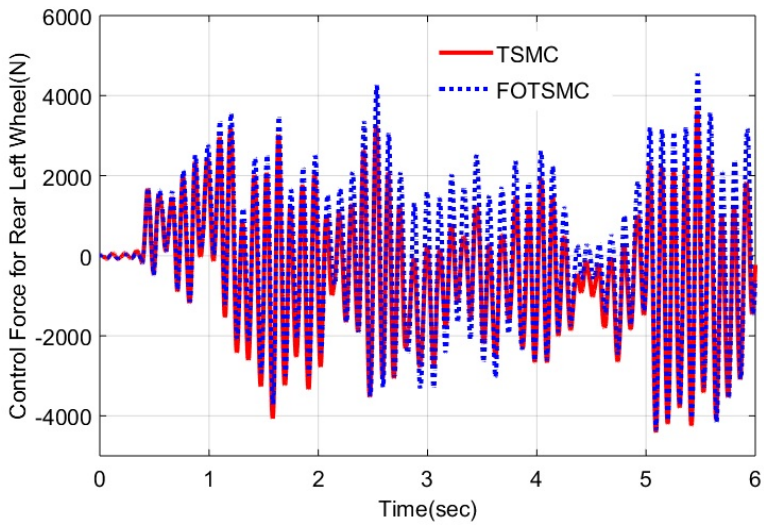

Figure 22: Force produced by the rear left actuator – RI

4.3. Analysis with Ride comfort as per ISO 2631

To investigate the ride comfort of the proposed FOTSMC strategy, the FWRMS [36] and Vibration Dose Value (VDV) [37] of BA are introduced to quantify the ride quality of the passenger as per ISO-2631. As seen from Table 3 and 4, FWRMS of BA for PSS, TSMC and FOTSMC are 0.5368 m/s^2, 0.05322 m/s^2 and 0.02374 m/s^2 respectively. Similarly 0.5529 m/s^2, 0.09723 m/s^2 and

0.08534 m/s^2 for RI. The ride comfort with PSS is 'Fairly Uncomfortable' (FU) which is improved to 'Not Uncomfortable' (NU) by TSMC and FOTSMC with BI. Also it is calculated for RI with PSS gives 'Little Uncomfortable' (LU) and enhanced to 'Not Uncomfortable' (NU) with TSMC and FOTSMC.

Table 3: Analysis with Ride comfort-BI

	FWRMS (m/s^2)	UL	VDV (m/s$^{1.75}$)
PASSIVE	0.537	FU	1.55
TSMC	0.053	NU	0.175
FOTSMC	0.024	NU	0.079

Table 4: Analysis with Ride comfort-RI

	FWRMS (rad/s^2)	UL	VDV (m/s$^{1.75}$)
PASSIVE	0.553	FU	1.097
TSMC	0.097	NU	0.199
FOTSMC	0.085	NU	0.169

4.4. Analysis with Sprung Mass variation

The sprung mass used for numerical simulation is 1500kg which includes the mass of the driver. As the driver mass may vary from 40 kg to 80 kg. Further analysis, the sprung mass is varied from 1460–1540 kg is considered. When the sprung mass decreases from 1500–1460 kg, percentage of reduction on RMS values of BA is decreased with TSMC and FOTSMC compared to PSS. Similarly when it increases from 1500–1540 kg, percentage of reduction on RMS values of BA is increased with TSMC and FOTSMC compared to PSS.

The maximum percentage of reduction in RMS values for 1540 kg with FOTSMC is 93.3% and with TSMC is 85.3%. Also it is tested for RI, the maximum percentage of reduction in RMS values for 1540 kg with FOTSMC is 53% and with TSMC is 49%. It is observed from the Figs. 23 and 24, the mass variation with BI and RI proves that percentage of reduction in RMS values increased with FOTSMC than TSMC.

When assessing intermittent vibration it is necessary to use the Vibration Dose Value (VDV), a cumulative measurement of the vibration level received over an 8-hour or 16-hour period. It is evaluated for BI and RI. It is concluded from the Tables 3 and 4, FOTSMC effectively reduces VDV of BA than TSMC and PSS.

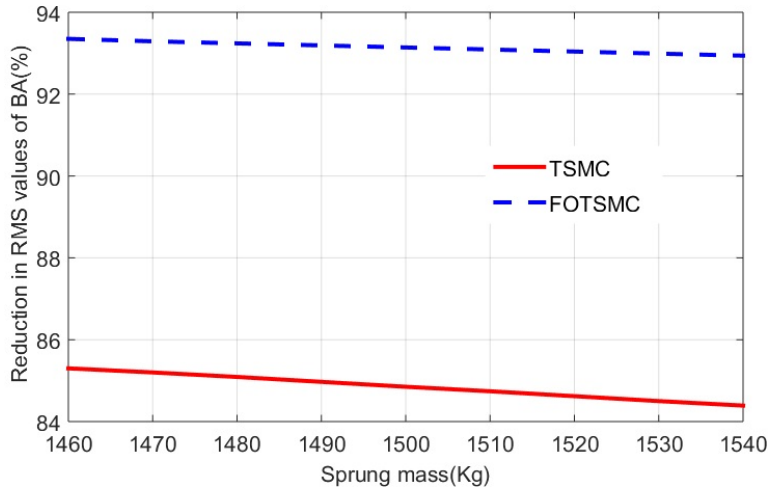

Figure 23: Performance of the SMCs with different mass – BI

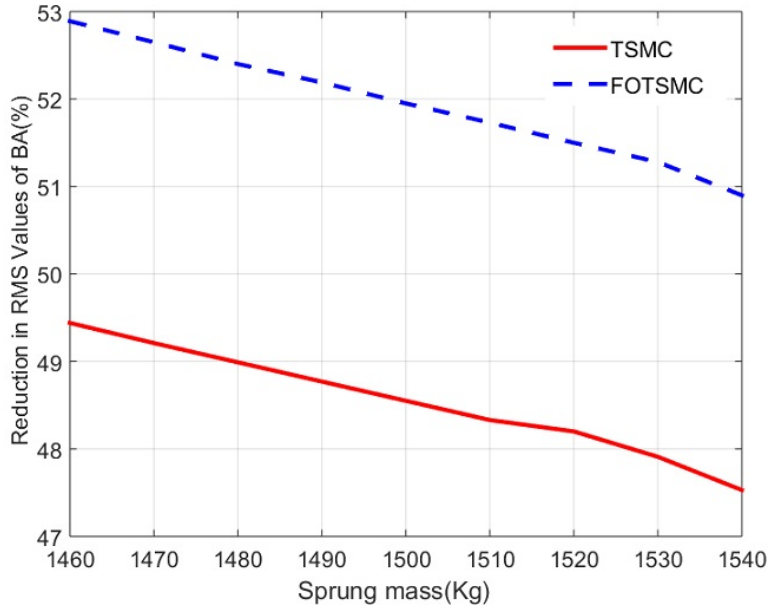

Figure 24: Performance of the SMCs with different mass – RI

4.5. Analysis with different speed

The BI and RI are designed with the speed of 30 kmph and the controller performances are tested. To show the robustness of the proposed controller, the speed is varied from 10–100 kmph and % of reduction in BA are computed and ploted.

It is seen from the Fig. 25, when the speed of the vehicle between 10–50 kmph, the percentage of reduction in RMS values of BA is maintained from 97–90% for FOTSMC and 89–80% for TSMC with BI. Similarly, speed variation is tested for RI, it shows that the changes in percentage of reduction for TSMC and FOTSMC. The FOTSMC performs better than TSMC which is shown in Fig. 26.

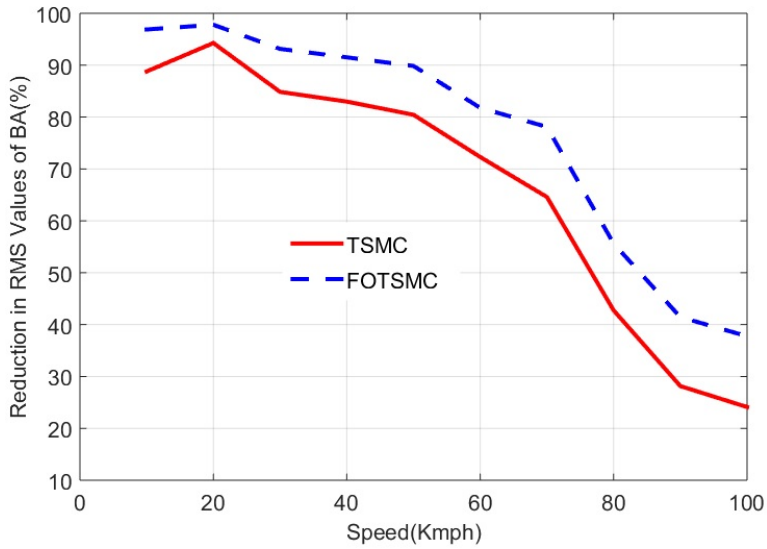

Figure 25: Performance of the SMCs with different speed – BI

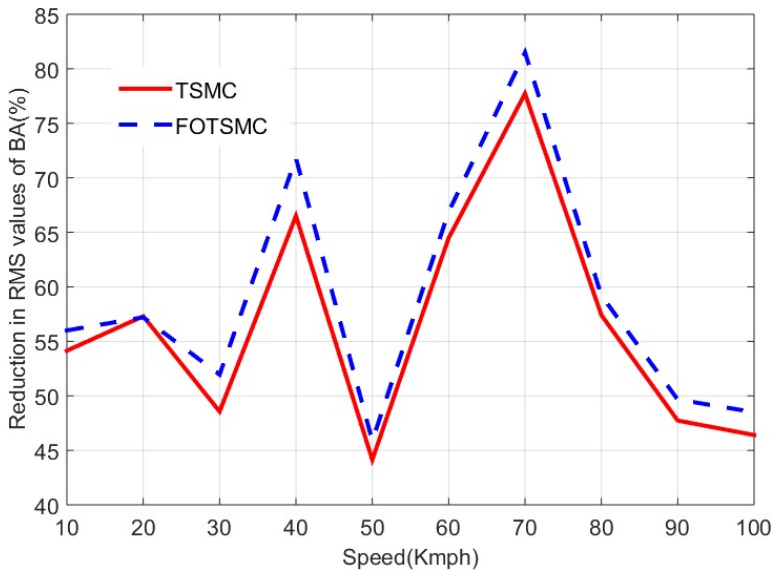

Figure 26: Performance of the SMCs with different speed – RI

4.6. Comparative analysis

The RMS values of BA with FOTSMC performs better than BA of existing Fuzzy SMC(FSMC) [13]. The numerical results proves that the RMS values of BA with BI and RI significantly reduced when it is compared to existing SMC. To evaluate the proposed controller performances, the percentage of reduction in RMS values of BA is calculated with respect to PSS. The proposed FOTSMC reduces the BA by 93.1% for BI and 52.3% for RI. The existing FSMC [17] decreases the BA by 34% with BI and 24% with RI. Therefore, FOTSMC performs better than existing FSMC. The comparison is made with existing SMC [33]. The RMS values of BA for existing SMC with BI are reduced to 83%, while for RI shows 49% of reduction in BA compared to PSS. The designed FOTSMC with BI reduces the RMS values of BA by 93% and 52.3% for RI. The comparative analysis of proposed FOTSMC with existing FSMC and SMC proves the effectiveness of the FOTSMC.

4.7. Stability analysis

The state variables such as suspension deflection and car body velocity of front left wheel for the TSMC and FOTSMC with BI and RI are plotted. The state trajectories of the TSMC and FOTSMC with BI are converging to the origin which is shown in Figs. 27 and 28. Hence the TSMC and FOTSMC for the BI are stable as per the Lyapunovs stability criteria.

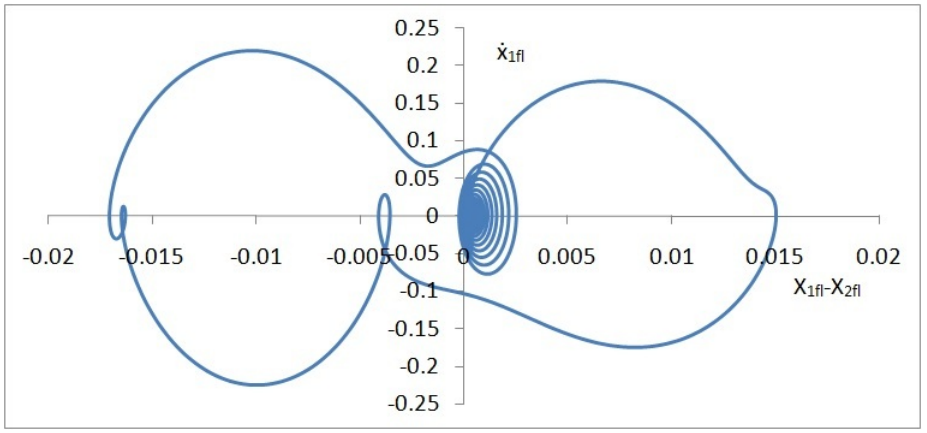

Figure 27: Phase plane of TSMC – BI

Definition 3.4 of the reference [38], An equilibrium point 0 is asymptotically stable if it is stable, and if in addition there exists some $r > 0$ such that $\|x(0)\| < r$ implies that $x(t) \to 0$ as $t \to \infty$. Asymptotic stability implies that the equilibrium point is stable, and the states are moving close to zero i.e converging to zero as time t tends to infinity. Figure 27 to 28 shows that system trajectories are converges to

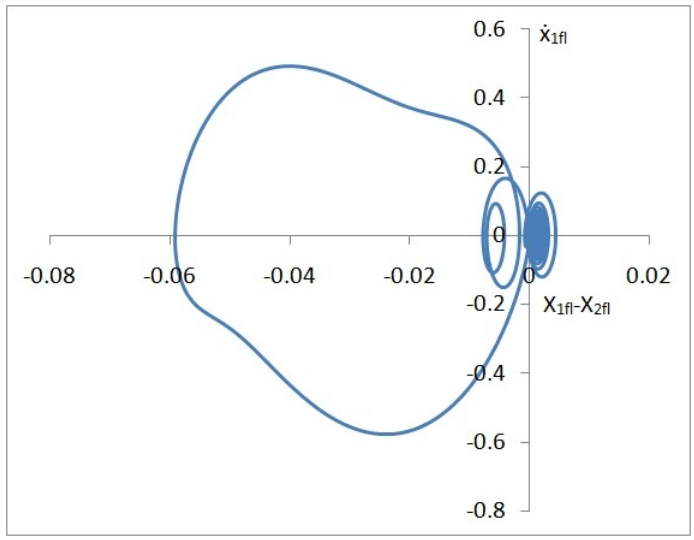

Figure 28: Phase plane of FOTSMC – BI

the origin for BI. For RI (Fig. 29 to 30), the system trajectories neither converge nor diverge to zero. An equilibrium point which is Lyapunov stable but not asymptotically stable is called marginally stable.

Also it is noted from the Figs. 29, 30 the state trajectories of the TSMC and FOTSMC with RI are neither converging to zero nor diverging to the infinity. It simply circles around the origin. Therefore the TSMC and FOTSMC are marginally stable as per the Lyapunovs stability criteria. Similarlly, the stability of

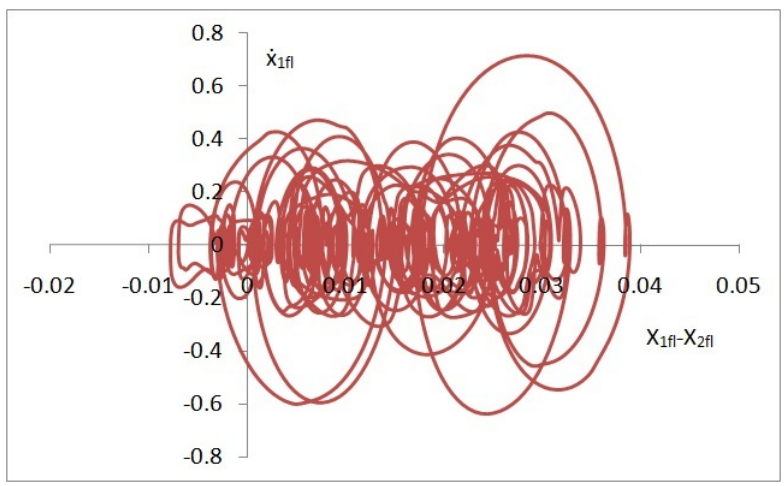

Figure 29: Phase plane of TSMC – RI

front right, rear left and rear right are asymptotically stable for BI and marginally stable for RI.

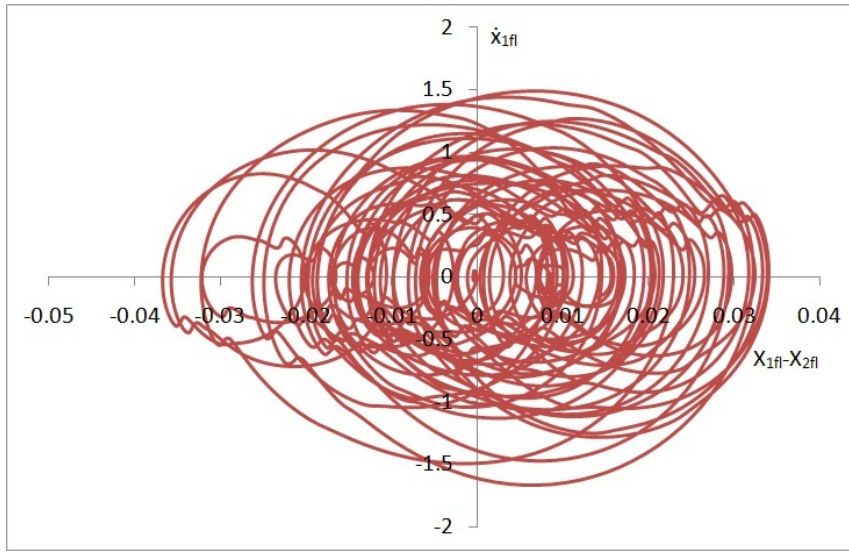

Figure 30: Phase plane of FOTSMC – RI

4.8. Power spectrum density analysis

The power spectrum density (PSD) of BA is plotted for BI and RI and it is shown in Figs. 31 and 32 respectively. It is observed from the two figures,

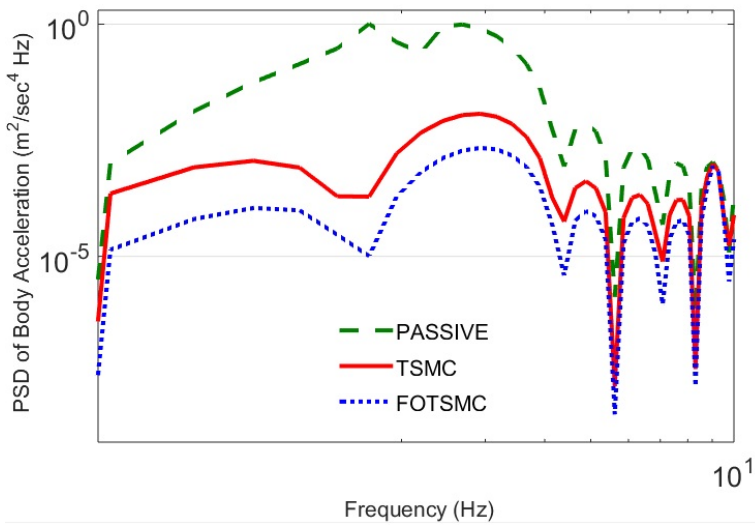

Figure 31: PSD of BA – BI

FOTSMC has reduced the BA which lies in the human sensitive frequency range of 4–8 Hz compared to TSMC and PSS.

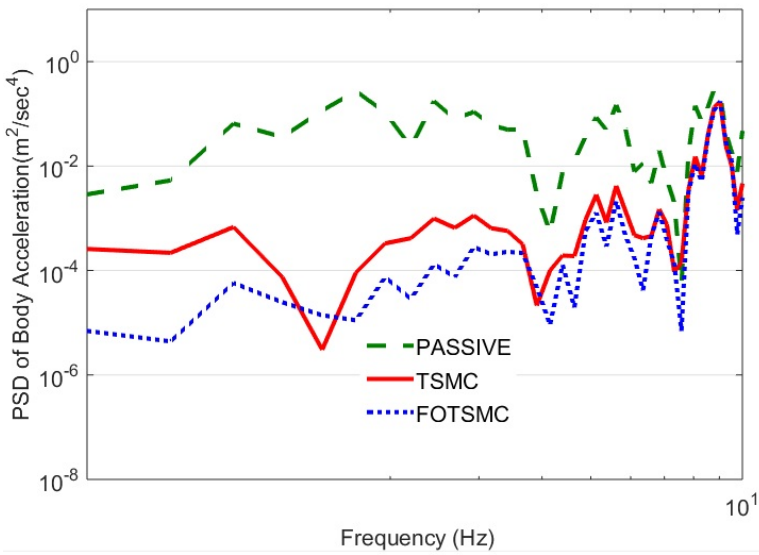

Figure 32: PSD of BA – RI

5. Conclusion

This paper is focused on designing FOTSMC for FCM and it is simulated by MATLAB/Simulink. The control strategies such as FOTSMC and TSMC are tested with BI and ISO-8608 RI. The percentage of RMS values and maximum peak overshoot for FOTSMC are significantly reduced compared to TSMC and PSS. To investigate the ride comfort of the passenger, FWRMS and VDV are computed for FOTSMC, TSMC and PSS. As per ISO-2631, the uncomfortable level and VDV is presented for BI and RI. The numerical results proves that FOTSMC and TSMC which enhances the ride comfort to 'Not Uncomfortable'. Also VDV is decreased in FOTSMC with BI and RI than TSMC and PSS. Also the designed controllers show that the Power Spectrum Density (PSD) of BA lies in the human sensitive range of 4–8 Hz for both BI and RI. The proposed FOTSMC is performs better than the existing FSMC and FOSMC. The numerical simulation proves that FOTSMC provides better ride comfort and decreases vibration level to zero. The robustness of the designed controllers are analysed for mass and speed variation with BI and RI. Further analysis with stability is carried out for TSMC and FOTSMC which guarantees the stability for TSMC and FOTSMC with BI and asymptotically stable for RI.

References

[1] Da-Shan Huang, Jin-Qiu Zhang, and Yi-Le Liu: The pid semi-active vibration control on nonlinear suspension system with time delay, *International Journal of Intelligent Transportation Systems Research*, 1–13, 2018.

[2] S. Kilicaslan: Control of active suspension system considering nonlinear actuator dynamics, *Nonlinear Dynamics*, **91**(2) (2018) 1383–1394.

[3] Zhi-Jun Fu, Bin Li, Xiao-Bin Ning, and Wei-Dong Xie: Online adaptive optimal control of vehicle active suspension systems using single-network approximate dynamic programming, *Mathematical Problems in Engineering*, 2017.

[4] Y. Abdulhammed and H. Elsherif: Development of a new automotive active suspension system, In *IOP Conference Series: Materials Science and Engineering*, volume 280, page 012024, IOP Publishing, 2017.

[5] S. Rajendiran, P. Lakshmi, and B. Rajkumar: Reduction of body acceleration in the quarter car model using fractional order fuzzy sliding mode controller, *International Journal of Vehicle Structures & Systems (IJVSS)*, **9**(2) (2017).

[6] H. Khodadadi and H. Ghadiri: Self-tuning pid controller design using fuzzy logic for half car active suspension system, *International Journal of Dynamics and Control*, **6**(1) (2018), 224–232.

[7] C.R. Hua, Y. Zhao, Z.W. Lu, and H. Ouyang: Random vibration of vehicle with hysteresis nonlinear suspension under road roughness excitation, *Advances in Mechanical Engineering*, **10**(1) (2018), 1687814017751222.

[8] Gang Wang, Changzheng Chen, and Shenbo Yu: Optimization and static output-feedback control for half-car active suspensions with constrained information, *Journal of Sound and Vibration*, **378** (2016), 1–13.

[9] Huihui Pan, Weichao Sun, Xingjian Jing, Huijun Gao, and Jianyong Yao: Adaptive tracking control for active suspension systems with non-ideal actuators, *Journal of Sound and Vibration*, **399** (2017), 2–20.

[10] Ch. Göhrle, A. Schindler, A. Wagner, and O. Sawodny: Road profile estimation and preview control for low-bandwidth active suspension systems, *IEEE/ASME Transactions on Mechatronics*, **20**(5) (2015), 2299–2310.

[11] K. Rajeswari and P. Lakshmi: Ga tuned distance based fuzzy sliding mode controller for vehicle suspension systems, *International Journal of Engineering and Technology*, **5**(1) (2008), 36–47.

[12] Yinlong Hu, Michael Z.Q. Chen, and Zhongsheng Hou: Multiplexed model predictive control for active vehicle suspensions, *International Journal of Control*, **88**(2) (2015), 347–363.

[13] Hung-Yi Chen and Shiuh-Jer Huang: A new model-free adaptive sliding controller for active suspension system, *International Journal of Systems Science*, **39**(1) (2008), 57–69.

[14] N. Yagiz and I. Yüksek: Robust control of active suspensions using sliding modes, *Turkish Journal of Engineering and Environmental Sciences*, **25**(2) (2001), 79–87.

[15] N.S. Bhangal and K.A. Raj: Fuzzy control of vehicle active suspension system, *International Journal of Mechanical Engineering and Robotics Research*, **5**(2) (2016), 144–148.

[16] M. Du, D. Zhao, B. Yang, and L. Wang: Terminal sliding mode control for full vehicle active suspension systems, *Journal of Mechanical Science and Technology*, **32**(6) (2018), 2851–2866.

[17] Chia-Ping Cheng, Chan-Hong Chao, and Tzuu-Hseng S. Li: Design of observer-based fuzzy sliding-mode control for an active suspension system with full-car model, In *Systems Man and Cybernetics (SMC), 2010 IEEE International Conference on*, pages 1939–1944, IEEE, 2010.

[18] Chia Ping Cheng and Tzuu-Hseng S. Li: Ep-based fuzzy control design for an active suspension system with full-car model, In *Systems, Man and Cybernetics, 2007, ISIC, IEEE International Conference on*, pages 3288–3293, IEEE, 2007.

[19] K.D. Young, V.I. Utkin, and U. Ozguner: A control engineer's guide to sliding mode control, In *IEEE International Workshop on Variable Structure Systems, 1996, Proceedings*, pages 1–14, IEEE, 1996.

[20] M. Moradi and A. Fekih: A stability guaranteed robust fault tolerant control design for vehicle suspension systems subject to actuator faults and disturbances, *IEEE Transactions on Control Systems Technology*, **23**(3) (2015), 1164–1171.

[21] Hui Pang, Xu Zhang, and Zeren Xu: Adaptive backstepping-based tracking control design for nonlinear active suspension system with parameter uncertainties and safety constraints, *ISA Transactions*, **88** (2019), 23–36.

[22] Hui Pang, Yan Wang, Xu Zhang, and Zeren Xu: Robust state-feedback control design for active suspension system with time-varying input delay

and wheelbase preview information, *Journal of the Franklin Institute*, **356**(4) (2019), 1899–1923.

[23] J. Mrazgua, T. El Houssaine, and M. Ouahi: Fuzzy fault-tolerant h_∞ control approach for nonlinear active suspension systems with actuator failure, *Procedia Computer Science*, **148** (2019), 465–474.

[24] A.P. Meran and Ü. Önen: Vibration analysis of a novel magnetic-viscous nonlinear passive isolator via finite element simulation, *Turkish Journal of Electrical Engineering and Computer Science*, **27**(3) (2019), 2309–2320.

[25] Jing Zhao, Pak Kin Wong, Zhengchao Xie, Xinbo Ma, and Xingqi Hua: Design and control of an automotive variable hydraulic damper using cuckoo search optimized pid method, *International Journal of Automotive Technology*, **20**(1) (2019), 51–63.

[26] Ahmed Shehata Gad, Helmy Mohamed El-Zoghby, Walid Abd El-Hady Oraby, and Samir Mohamed El-Demerdash: Performance and behaviour of a magneto-rheological damper in a semi-active vehicle suspension and power evaluation, *American Journal of Mechanical Engineering and Automation*, **5**(3) (2018), 72–89.

[27] W. Sun, H. Gao, and B. Yao: Adaptive robust vibration control of full-car active suspensions with electrohydraulic actuators, *IEEE Transactions on Control Systems Technology*, **21**(6) (2013), 2417–2422.

[28] N. Zhang, L. Wang, and H. Du: Motion-mode energy method for vehicle dynamics analysis and control, *Vehicle System Dynamics*, **52**(1) (2014), 1–25.

[29] P. Gáspár, I. Szaszi, and J. Bokor: Design of robust controllers for active vehicle suspension using the mixed μ synthesis, *Vehicle system dynamics*, **40**(4) (2003), 193–228.

[30] R. Darus and Y.M. Sam: Modeling and control active suspension system for a full car model, In *Signal Processing & Its Applications, 2009. CSPA 2009, 5th International Colloquium on*, pages 13–18, IEEE, 2009.

[31] C. Kim and P.I. Ro: An accurate full car ride model using model reducing techniques, *Journal of Mechanical Design*, **124**(4) (2002), 697–705.

[32] Zifan Fang, Wenhui Shu, Daojia Du, Bingfei Xiang, Qingsong He, and Kongde He: Semi-active suspension of a full-vehicle model based on double-loop control, *Procedia Engineering*, **16** (2011), 428–437.

[33] T. Yuvapriya, P. Lakshmi, and S. Rajendiran: Vibration suppression in full car active suspension system using fractional order sliding mode controller, *Journal of the Brazilian Society of Mechanical Sciences and Engineering*, **40**(4) (2018), 217–226.

[34] V. Behnamgol and A.R. Vali: Terminal sliding mode control for nonlinear systems with both matched and unmatched uncertainties, *Iranian Journal of Electrical & Electronic Engineering*, **11**(2) (2015), 109.

[35] S. Rajendiran, P. Lakshmi, and B. Rajkumar: Enhancing travel comfort of quarter car with driver model using fractional order terminal sliding mode controller with dual actuator, *Journal of Electrical Engineering*, **16**(4) (2016), 203–214.

[36] A. Kuznetsov, M. Mammadov, I. Sultan, and E. Hajilarov: Optimization of improved suspension system with inerter device of the quarter-car model in vibration analysis, *Archive of Applied Mechanics*, **81**(10) (2011), 1427–1437.

[37] Maria Lúcia Machado Duarte, Priscila Albuquerque de Araújo, Frederico Catone Horta, Sara Del Vecchio, and Lucas Augusto Penna de Carvalho: Correlation between weighted acceleration, vibration dose value and exposure time on whole body vibration comfort levels evaluation, *Safety Science*, **103** (2018), 218–224.

[38] J.-J.E. Slotine and W. Li: *Applied nonlinear control*, volume 199. Prentice hall Englewood Cliffs, NJ, 1991.